Journal of Inorganic Biochemistry 128 (2013) 26–37

Contents lists available at SciVerse ScienceDirect

Journal of Inorganic Biochemistry

journal homepage: www.elsevier.com/locate/jinorgbio

# Synthesis, characterization and cell viability test of six vanadyl complexes with acetylacetonate derivatives

Speranza Sgarbossa [a], Eliano Diana [a], Domenica Marabello [a], Annamaria Deagostino [a], Silvano Cadamuro [a], Alessandro Barge [b], Enzo Laurenti [a], Margherita Gallicchio [b], Valentina Boscaro [b], Elena Ghibaudi [a,*]

[a] Dip.to di Chimica, University of Torino, Via Giuria 7, I-10125 Torino, Italy
[b] Dip.to di Scienza e Tecnologia del Farmaco, University of Torino, Via Giuria 9, I-10125 Torino, Italy

ARTICLE INFO

*Article history:*
Received 11 April 2013
Received in revised form 3 July 2013
Accepted 8 July 2013
Available online 18 July 2013

*Keywords:*
Vanadyl compounds
Antitumoral metal complexes
Acetylacetonate derivatives
X-ray crystallography
EPR spectroscopy
Vibrational spectroscopy

ABSTRACT

Vanadium compounds are known to display a number of therapeutic effects, namely insulin-mimetic and cardiovascular effects. Evidence of the antiproliferative and proapoptotic activity of a number of vanadyl complexes, together with their low toxicity, establishes these metal compounds as promising antitumoral therapeutic agents. In the present work, we describe the synthesis and full characterization of six new vanadyl complexes with acetylacetonate derivatives bearing asymmetric substitutions on the β-dicarbonyl moiety: the complexes were characterized in the solid state as well as in solution. Our results show that all complexes are in square pyramidal geometry; *cis* isomers in the equatorial plane are favored in the presence of strongly coordinating solvents. EPR evidence suggests that all complexes are in the bis-chelate form, although in two cases the mono-chelated complex seems to be present as well. Preliminary tests carried out on non-tumor and tumor cell lines show that these complexes are effective in suppressing cell viability and elicit a distinct response of tumor and non-tumor cells.


## 1. Introduction

Vanadium compounds have been shown to display several therapeutic effects, including insulin-mimetic, cardiovascular, anticarcinogenic, antiproliferative and proapoptotic effects [1,2]. In particular, the antitumoral properties of vanadium complexes raise attention due to the relatively low toxicity of vanadium compounds [2].

A number of vanadyl complexes have been synthesized and investigated relatively to their application in anticancer therapies [3,4]: they include vanadocene derivatives [5] and many complexes of the $VO^{2+}$ moiety with organic ligands (Schiff bases, phenanthroline and quinoxaline derivatives, etc.) that may interact with DNA and other cellular targets [6].

The vanadyl complex with pentane-2,4-dionato (acetylacetonate, acac) is one of the oldest vanadium therapeutic agent ever synthesized [7]. Apart from its insulin-mimetic activity [8,9], more recent studies [9,10] have highlighted its anticancer potential on human hepatoma cell line. Although the molecular details of such effect are not clear, $[VO(acac)_2]$ has been shown to display several actions: it is an efficient DNA cleaving agent at submicromolar concentration [8]; it has been found more effective than vanadyl sulphate in stimulating the activity of a cytosolic protein kinase [11,12], blocking cell cycle progression at G1 phase [10] and inducing mitochondrial toxicity through oxidative stress mechanisms [13]. In addition, $[VO(acac)_2]$ was proposed as the structural basis for a new class of cancer-specific MRI contrast agents that are non-toxic and highly sensitive to cancer metabolism [1,14].

A variety of vanadyl complexes with acac-derivatives (β-dicarbonyl ligands) have been reported [15] and shown to display anticancer activity [16]: e.g. the [VO(curcumin)] complex was found able to inhibit mouse lymphoma cell growth [17].

Due to these reasons, vanadyl complexes with ligands bearing symmetric and asymmetric substitutions on the β-dicarbonyl moiety have raised a strong interest [15,18] and their behavior in terms of pharmacological and structural properties deserves to be investigated. In fact, highlighting the structure–function relationships of this class of compounds is crucial for designing new pharmacologically-active molecules and unraveling the molecular targets of these species.

A crucial issue related with vanadyl complexes with acac-derivatives concerns their behavior in solution, as these compounds may interact with solvents, giving rise to a wide range of chemical species with distinct pharmacological effects [19].

Whereas these complexes in the solid state display a square pyramidal geometry with the oxo-ligand in the axial position and the two β-dicarbonyl ligands in the equatorial plane [20,21], upon dissolution in organic solvents they may interact with solvent molecules via hydrogen bonding or by direct coordination to the sixth vacant site of the transition metal ion, leading to $[VO(acac)_2L]$ adducts (L = coordinating solvent molecule) [15,19]. *Cis*/*trans* isomers in the equatorial plane may form in the presence of ligands bearing

* Corresponding author. Tel.: +39 11 6707951; fax: +39 11 6707855.
*E-mail address:* elena.ghibaudi@unito.it (E. Ghibaudi).

0162-0134/$ – see front matter © 2013 Elsevier Inc. All rights reserved.
http://dx.doi.org/10.1016/j.jinorgbio.2013.07.015

asymmetric substitutions on the β-dicarbonyl moiety (we will refer to as *cis*-planar and *trans*-planar isomers); in addition, depending on the nature of the solvent, the L ligand may lie either in the equatorial plane (*cis* to the VO moiety) or occupy the 6th coordination position (*trans* to the VO moiety) [22]. The concerted use of different spectroscopical techniques may help to discriminate between the species found in solution.

In the present work, we present the synthesis and characterization of six new vanadyl complexes with acac-ligand derivatives. The species in the solid state were characterized by X-ray crystallography and Raman spectroscopy; a combination of EPR and optical spectroscopy was employed to characterize the species in solution. Preliminary in vitro tests performed on different cell lines (HCT 116, HT-29, hTERT-HME1 and human immortalized podocytes) have shown specific cell toxicity of some complexes and establish these compounds as potential antitumoral agents.

## 2. Experimental

All commercially obtained reagents and solvents were used as received. Products were purified by a preparative column chromatography on Macherey Nagel silica-gel for flash chromatography, 0.04–0.063 mm/230–400 mesh. Reactions were monitored by TLC using silica-gel on TLC-PET foils (Fluka), 2–25 μm, layer thickness 0.2 mm, medium pore diameter 60 Å.

The synthesis of the ligands was performed according to the protocol described by Li and coworkers [23] and modified by the authors.

In a 250 mL round bottom flask the ethyl trifluoroacetate (10.37 g, 73.0 mmol) and the suitable ketone (33.0 mmol) were dissolved in a 21% solution of EtONa (73.0 mmol) in EtOH. The reaction mixture was stirred at 70 °C until disappearance (3–4 h) of the ketone spot at TLC ($CH_2Cl_2$/MeOH 95/5 v/v). Then the solvent was evaporated, and the solid residue was dissolved with $H_2O$, acidified with HCl 6 N until pH 3–4. Then it was extracted with $CH_2Cl_2$ (2 × 20 mL), dried over $Na_2SO_4$, filtered and evaporated under reduced pressure, to give the crude reaction product that was purified by chromatography ($CH_2Cl_2$/MeOH 95/5 v/v).

*N*-methyl-3-acetylindole was synthesized following the procedure reported in literature and the spectral data corresponded to those reported in the literature [24]. Ligands 1-(2-naphtyl)-4,4,4-trifluorobutane-1,3-dione (ligand **c**) and 1-(3-thienyl)-4,4,4-trifluorobutane-1,3-dione (ligand **f**) were purchased from Sigma Aldrich.

The synthesis of the vanadyl complexes was performed according to the protocol described by Li and coworkers [23] and modified by the authors.

A 2-fold molar excess of the ligand dissolved in 2 mL EtOH was mixed with vanadyl sulphate (60 mg) dissolved in 1.5 mL $H_2O$. The solution was kept under stirring and basified with diluted ammonia ($NH_3$/$H_2O$ 1/10 v/v) until a precipitate appeared. After centrifugation, the precipitate was recrystallized in EtOH at 4 °C.

### 2.1. Ligand **a**) 1-phenyl-4,4,4-trifluorobutane-1,3-dione

Following the above-described procedure, acetophenone (4.0 g, 33.0 mmol) was treated with ethyl trifluoroacetate and EtONa in EtOH affording a pale yellow solid (4.28 g, 60% — petroleum ether/ethyl ether 90/10 v/v, 10% formic acid). Found C, 55.60; H, 3.27, F, 26.33%. Calc. for $C_{10}H_7F_3O_2$: C, 55.56; H, 3.26, F, 26.37%. $\nu_{max}$(neat)/$cm^{-1}$ 1602. $\delta_H$ (200 MHz; $CDCl_3$, $Me_4Si$) 6.59 (1H, s, C═C*H*), 7.60 (3H, m, Ar), 8.10 (2H, m, Ar); $\delta_C$ (50.2 MHz; $CDCl_3$, $Me_4Si$) 91.9 (1 × d), 117.1 (q, *J*(CF) = 281 Hz), 126.9 (2 × d), 128.7 (2 × d), 132.5 (1 × s), 133.2 (1 × d), 176.9 (q, *J*(CF) = 36.5 Hz), 186.0 (1 × s). Mass spectrometry (MS) (Electronic impact (EI), 70 eV): *m/z* (%) = 216 (76, $M^+$), 147 (100), 69 (94); m.p. 37.8 °C–39 °C.

### 2.2. Ligand **b**) 1-(4-methoxyphenyl)-4,4,4-trifluorobutane-1,3-dione

Following the above-described procedure, *p*-methoxyacetophenone (4.95 g, 33.0 mmol) was treated with ethyl trifluoroacetate and EtONa in EtOH affording a pale yellow solid (4.79 g, 59% — petroleum ether/ethyl ether 90/10 v/v, 10% formic acid). Found C, 53.69; H, 3.70, F, 22.99%. Calc. for $C_{11}H_9F_3O_3$: C, 53.67; H, 3.68, F, 23.15%. $\nu_{max}$(neat)/$cm^{-1}$ 1600. $\delta_H$ (200 MHz; $CDCl_3$, $Me_4Si$) (2H, d, C═C*H*), 3.91 (3H, s, $OCH_3$), 6.52 (1H, s, C═C*H*), 7.00 (2H, d, *J* = 8.0 Hz, Ar), 7.94 (2H, d, *J* = 8.0 Hz, Ar); $\delta_C$ (50.2 MHz; $CDCl_3$, $Me_4Si$) 55.1 (1 × q), 91.1 (1 × d), 114.1 (2 × d), 117.1 (q, *J* (CF) = 300.5 Hz), 124.9 (1 × s), 129.7 (2 × d), 164.5 (1 × d), 175.3 (q, *J* (CF) = 35.5 Hz), 186.0 (1 × s). MS (EI, 70 eV): *m/z* (%) = 246 (97, $M^+$), 177 (100), 69 (54); m.p. 60.0 °C–60.1 °C.

### 2.3. Ligand **d**) 1-(6-methoxy-2-naphtyl)-4,4,4-trifluorobutane-1,3-dione

Following the above-described procedure, 6-methoxy-2-acetonaphtone (6.60 g, 33.0 mmol) was treated with ethyl trifluoroacetate and EtONa in EtOH affording a brilliant yellow solid (8.50 g, 87% — $CH_2Cl_2$/MeOH 95/5 v/v). Found C, 61.00; H, 3.70, F, 19.20%. Calc. for $C_{15}H_{11}F_3O_3$: C, 60.82; H, 3.74, F, 19.24%. $\nu_{max}$(neat)/$cm^{-1}$ 1628. $\delta_H$ (200 MHz; $CDCl_3$, $Me_4Si$) (2H, d, C═C*H*), 3.97 (3H, s, $OCH_3$), 6.70 (1H, s, C═C*H*), 7.32 (2H, m, Ar), 7.89 (3H, m, Ar) 8.44 (1H, bs, Ar); $\delta_C$ (50.2 MHz; $CD_3COCD_3$, $Me_4Si$) 54.8 (1 × q), 92.3 (1 × d), 105.8 (1 × d), 117.4 (q, *J* (CF) = 280.0 Hz), 119.8 (1 × d), 123.3 (1 × d), 127.4 (1 × d), 127.8 (2 × s), 130.6 (1 × d), 131.2 (1 × d), 138.0 (1 × s), 160.4 (1 × s), 174.8 (q, *J* (CF) = 35.0 Hz), 187.2 (1 × s). MS (EI, 70 eV): *m/z* (%) = 296 (100, $M^+$), 227 (45), 69 (38); m.p. 92.5 °C–920.7 °C.

### 2.4. Ligand **e**) 1-(N-methyl-3-indolyl)-4,4,4-trifluorobutane-1,3-dione

Following the above-described procedure, *N*-methyl-3-acetylindole (5.71 g, 33.0 mmol) was treated with ethyl trifluoroacetate and EtONa in EtOH affording a brilliant yellow solid (6.30 g, 71% — $CH_2Cl_2$/MeOH 95/5 v/v). Found C, 58.09; H, 3.81, F, 21.24, N 5.28 %. Calc. for $C_{13}H_{10}F_3NO_2$: C, 58.00; H, 3.74, F, 21.17, N 5.20 %. $\nu_{max}$(neat)/$cm^{-1}$ 1628. $\delta_H$ (200 MHz; $CDCl_3$, $Me_4Si$) (2H, d, C═C*H*), 3.92 (3H, s, $NCH_3$), 6.38 (1H, s, C═C*H*), 7.38 (3H, m, Ar), 7.89 (1H, s, N–CH) 8.25 (1H, m, Ar); $\delta_C$ (50.2 MHz; $CD_3COCD_3$, $Me_4Si$) 33.1 (1 × q), 93.2 (1 × d), 110.7 (1 × d), 111.8 (1 × s), 118.0 (q, *J* (CF) = 300.5 Hz), 121.8 (1 × d), 122.8 (1 × d), 123.7 (1 × d), 125.6 (1 × s), 138.1 (1 × s), 138.4 (1 × s), 168.0 (q, *J* (CF) = 35.0 Hz), 186.1 (1 × s). MS (EI, 70 eV): *m/z* (%) = 269 (100, $M^+$), 200 (61), 132 (53); m.p. 125.9 °C–126.2 °C.

$^1$H NMR spectra were recorded at 200 MHz or 300 MHz on a Bruker spectrometer, and $^{13}$C NMR spectra at 50.2 MHz, in $CDCl_3$.

Data were reported as follows: chemical shifts in ppm from $Me_4Si$ as an internal standard, integration, multiplicity, coupling constants (Hz), and assignments. $^{13}$C NMR spectra were measured with complete proton decoupling. Chemical shifts were reported in ppm from the residual solvent peak as an internal standard. GC-MS spectra were obtained on a mass selective detector HP 5970 B instrument operating at an ionizing voltage of 70 eV connected to a HP 5890 GC with a cross linked methyl silicone capillary column (25 m × 0.2 mm × 0.33 μm film thickness).

ESI-MS spectra were recorded on a Waters Micromass ZQ instrument equipped with ESCi source. MS analyses of the complexes were carried out in the ESI + modality. Each vanadyl complex was dissolved in a $d^6$-DMSO solution, diluted in methanol/water (9:1 v/v) + formic acid 0.1% v/v, and injected in the ESI source.

IR spectra of ligands and complexes (in the solid state) were recorded on a PerkinElmer BX FT-IR and a Bruker Vertex 70 spectrophotometer, equipped with RAM-II module. FT-IR was measured by using an anvil ATR cell. Laser wavelength of the Raman module is 1064 nm.

DFT calculations were performed by using the hybrid B3LYP functional and the 6-311g(d,p) basis set for all elements, by means of Gaussian 09 package [25].

Optical spectra of the complexes dissolved in acetone, methanol and DMSO were recorded on a double-beam UVICAM300 spectrophotometer (ThermoSpectronic). All solvent were bubbled with argon for 15 min, in order to remove oxygen.

77 K EPR spectra of saturated solution of each complex in acetone were recorded on a CW-EPR spectrometer ESP300E (Bruker) equipped with a cylindrical cavity. Experimental settings were as follows: microwave frequency ~9.5 GHz; modulation frequency 100 KHz; modulation amplitude 4 G; microwave power 2 mW; and time constant 163 ms. All spectra were simulated with the EPRSim32.03 software [26] whose spin Hamiltonian takes into account second order effects typical of vanadyl systems.

X-ray crystal structures were determined according to the following procedure.

For all compounds the intensity data were collected at 153 K on an Oxford Diffraction Gemini R-Ultra diffractometer equipped with nitrogen low temperature device and Enhanced Ultra (Cu) X-ray Source (Agilent Technologies). The intensities were corrected for absorption with the numerical correction based on Gaussian integration over a multifaceted crystal model. Software used: CrysAlisPro (Agilent Technologies, Version 1.171.36.20 (release 27-06-2012 CrysAlis171.NET, compiled Jul 11 2012,15:38:31) for data collection, data reduction and absorption correction; SHELXTL(Sheldrick M. (1997), SHELXTL, Version 5.1, Bruker AXS inc., Madison) for data solution, structure analysis and drawing preparation; SHELXL-2012 (Sheldrick M. (2012), SHELXL-2012) for refinement. Details of crystal data, data collection and refinement parameters are given in Table 1S. Crystallographic data (without structure factors) for the structure(s) reported in this paper have been deposited with the Cambridge Crystallographic Data Centre (CCDC) as supplementary publication nr. CCDC 930935 (complex **e**-ACETONE), CCDC 930936 (complex **e**-DMSO), CCDC 930937 (complex **f**), CCDC 930938 (complex **b**). Copies of the data can be obtained free of charge from the CCDC (12 Union Road, Cambridge CB2 1EZ, UK; Tel.: +44-1223-336408; Fax: +44-1223-336003; e-mail: deposit@ccdc.cam.ac.uk; Web site: http://www.ccdc.cam.ac.uk).

Crystals suitable for X-ray analysis were obtained at room temperature, by slow evaporation of the solvent, dimethylformamide for complex **b**, dimethylsulfoxide for complexes **f** and **e**-DMSO, and acetone for complex **e**-ACETONE. The intensity data were collected using graphite-monochromatized Mo-Kα radiation (λ = 0.71073 Å) for compound **b** and mirror monochromatized Cu-Kα radiation (λ = 1.5418 Å) for **f**, **e**-DMSO and **e**-ACETONE. All non-hydrogen atoms were anisotropically refined, except for the DMSO-free molecule of complex **f**, the C and O atoms of the free disordered DMSO molecules of complex **e**-DMSO and the disordered $CF_3$ groups in complex **e**-ACETONE. Hydrogen atoms were calculated and refined riding with $U_{iso}$ = 1.2 or 1.5 $U_{eq.}$ or of the carbon atom connected.

In vitro cell tests were performed on the following cell lines: HCT 116, HT-29, and hTERT-HME1.

HCT 116, HT-29, and hTERT-HME1 were purchased from the American Type Culture Collection; immortalized human podocytes were kindly provided by Prof. Gianluca Miglio (University of Torino, Dip.to Scienza e Tecnologia del Farmaco).

HCT 116, HT-29 and podocytes were cultured in DMEM medium (Sigma-Aldrich) supplemented with 10% fetal bovine serum (PAA Laboratories GmbH). hTERT-HME1 cells were grown in DMEM-F12 medium (Sigma-Aldrich), supplemented with 2% fetal bovine serum, 20 ng/mL EGF, 10 g/mL insulin, and 100 g/mL hydrocortisone. All cell culture media were supplemented with 50 units/mL penicillin and 50 mg/mL streptomycin.

All vanadyl compounds and ligands were dissolved in DMSO and $VOSO_4$ in the appropriate medium.

Cells were seeded in 100 μL complete medium at appropriate density (1500–2000 cells/well) in 96-well plastic culture plates in triplicate. The following day, after serial dilutions, 100 μL of each compound, ligand and $VOSO_4$ in serum-free medium were added to cells with a multichannel pipette. Vehicle and medium-only containing wells were added as controls. Plates were incubated at 37 °C in 5% $CO_2$ for 6 days, after which cell viability was assessed by ATP content using the CellTiter-Glo Luminescent Assay (Promega). All luminescence measurements (indicated as relative light units) were recorded on a Victor X5 multimode plate reader (PerkinElmer).

## 3. Results

Fig. 1 reports the structural formulas of six new vanadyl complexes that were synthesized either using commercially available acac-derivatives or ligands synthesized by the authors.

### 3.1. Synthesis and NMR/MS characterization of the ligands and the complexes

Ligands for complexes **a**, **b**, **d**, **e** were synthesized in good yields (**a**: 60%; **b**: 59%; **d**: 87%; **e**: 71%) through a Claisen condensation applied to ethyl trifluoroacetate and phenyl-, indolyl-, or 2-naphtyl etanone derivatives. The methoxy electron donor substituent was introduced both on the phenyl and naphthyl rings at positions 4 and 6, respectively. All the ligands were purified and fully characterized (Supplementary material, Figs. 1S–5S).

These ligands were subsequently employed for the synthesis of vanadyl complexes **a**–**f** according to the protocol described in the Experimental section. The formation of each complex was monitored by MS and NMR spectroscopy.

$^1$H NMR spectra of complexes **a**–**f** highlight the $VO^{2+}$ paramagnetic effect on the ligand resonances that results in line broadening (due to enhanced spin relaxation) without affecting their chemical shifts to a significant extent as already reported for the [$VO(acac)_2$] complex and its derivatives [16,27,28]. Line broadening is taken as an evidence of complexation, although the invariancy of chemical shift prevents the extrapolation of any information on the geometry of the complex (Fig. 2, upper and lower spectra).

The pseudomolecular ions ($M + H^+$) and the complex adducts with sodium and potassium ($M + Na^+$, $M + K^+$), where M refers to the $VO^{2+}$ complex with two acac-derived ligands, were detected by MS analyses of complexes **a**–**f** in the ESI+ modality. In addition, signals assignable to $VO^{2+}$ associated with a single ligand molecule and one or two DMSO molecules were found (Supplementary material, Figs. 6S–11S). The replacement of ligands **a**–**f** with DMSO can be explained by taking into account the protonation effect of formic acid onto the enolate ion that suppresses the coordination ability of the ligand and allows ligand exchange. This process certainly occurs inside the MS source, although it cannot be excluded that similar events occur in solution or inside cells. $^1$H NMR spectra, recorded in acetone or DMSO, do not highlight the presence of significant amounts of free ligands, which would be expected as a result of the dissociation process although, this evidence does not rule out the possibility of dissociation processes occurring on small amounts of the complexes.

### 3.2. X-ray crystal structure analysis

In order to characterize the structure of complexes **a**–**f** in the solid state, several crystallization attempts of these compounds were made in different solvents. Finally, crystals suitable for X-ray analysis were obtained by slow evaporation of the solvent at room temperature, for complex **b** (in DMF), complex **f** (in DMSO) and complex **e** (in DMSO and acetone that we refer to as **e**-DMSO and **e**-ACETONE, respectively). Their molecular structures with atom labeling are reported in Fig. 3.

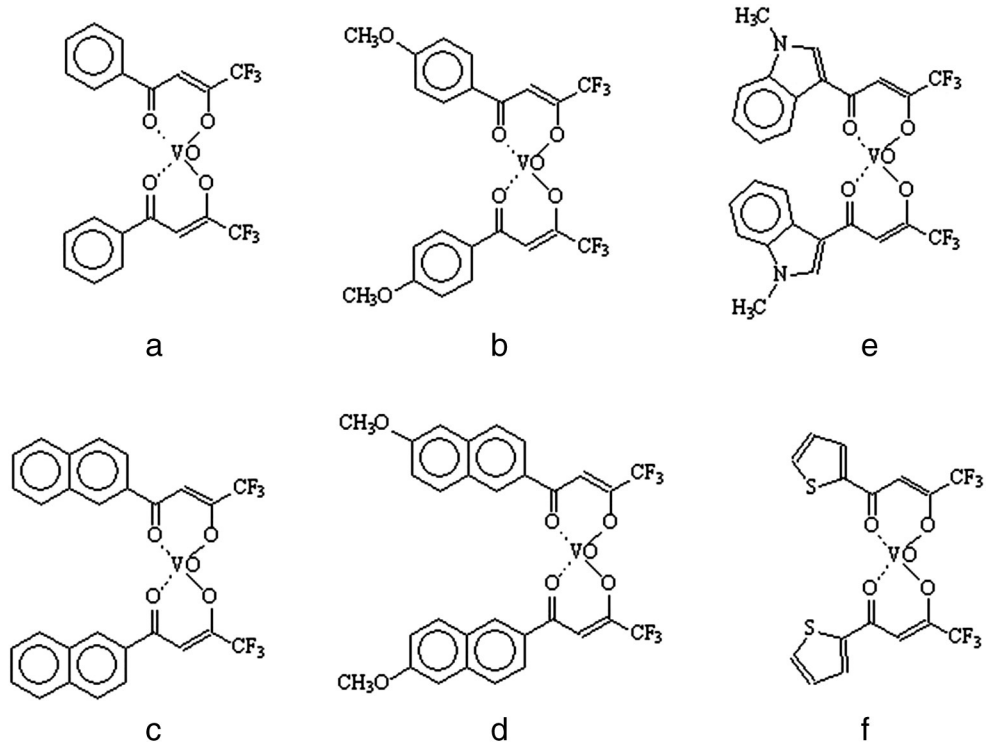


**Fig. 1.** Structural formulas of complexes **a**–**f**: a) 1-phenyl-4,4,4-trifluorobutane-1,3-dione; b) 1-(4-methoxyphenyl)-4,4,4-trifluorobutane-1,3-dione; c) 1-(2-naphtyl)-4,4,4-trifluorobutane-1,3-dione; d) 1-(6-methoxy-2-naphtyl)-4,4,4-trifluorobutane-1,3-dione; e) 1-(*N*-methyl-3-indolyl)-4,4,4-trifluorobutane-1,3-dione; f) 1-(3-thienyl)-4,4,4-trifluorobutane-1,3-dione.

In all cases, except complex **e**-ACETONE, a strongly distorted octahedral geometry was found, with two 1,3-carbonyl units coordinated to the metal center in the equatorial positions and the two axial coordination sites occupied by the vanadyl oxygen and a solvent molecule, respectively. Conversely, complex **e**-ACETONE does not coordinate the solvent and showed the typical square pyramidal geometry already found in similar complexes [20,21], with the VO moiety in the apical position and the two β-dicarbonyl ligands in the square base.

The relative orientation of the $CF_3$ moieties in the ligands shows that complexes **b**, **f** and **e**-DMSO are *cis-planar* isomers while the **e**-ACETONE complex is *trans-planar*.

The asymmetric unit of complex **b** contains one compound molecule (Fig. 3) with one solvent molecule coordinated to the vanadium atom. The two rings formed by complexation of the metal atom by the 1,3-carbonyl ligands are almost planar (the mean deviation from planarity is 0.030 for ring A [V(1) – O(2A) – C(2A) – C(3A) – C(4A) – O(3A)] and 0.009 for ring B [V(1) – O(2B) – C(2B) – C(3B) – C(4B) – O(3B)]). The carbonyl units are bent towards the coordinated DMF molecule (the angles between the V(1) – O(1) bond and rings A and B are 98.3° and 91.8°, respectively), likely due to the great repulsion exerted by the vanadyl–oxygen electron couplets on the four equatorial carbonyl oxygens. In the β-dicarbonyl ligands, a slight rotation of the phenyl rings is observed (the angle between ring A and the phenyl ring C(5A) – C(10A) is 7.8°, whereas the angle between ring B and the phenyl ring C(5B) – C(10B) is 3.2°), probably due to crystal packing; this rotation is too small to prevent delocalization of charge density through the ligands, as witnessed by the lower C(4) – C(5) distance (1.478(4) Å av.) with respect to a typical localized single bond.

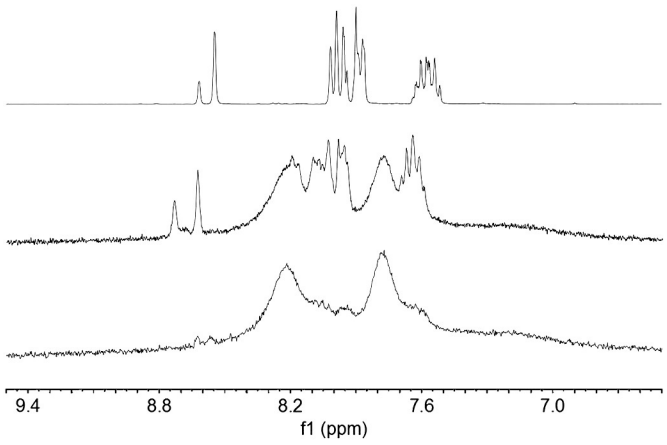


**Fig. 2.** Magnified aromatic region of the $^1$H NMR spectra in methanol d$^4$ of ligand c (upper spectrum), freshly dissolved complex c (lower spectrum) and complex c after 5 day incubation at room temperature (middle spectrum).

In the case of complex **f**, the asymmetric unit contains one compound molecule with a solvent molecule coordinated to the vanadium atom and one free DMSO molecule. Once again, the two rings formed by complexation of the metal atom by the 1,3-carbonyl ligands are almost planar (mean deviation from planarity is 0.013 for ring A and 0.012 for ring B) and the carbonyl units are more bent towards the coordinated DMSO molecule (the angles between the V(1) – O(1) bond and the rings A and B are 100.9° and 100.8° respectively) with respect to complex **b**. The thiophene moieties are slightly rotated with respect to the 1,3-carbonyl rings (the angle between ring A and the thiophene moiety C(5A) – S(9A) is 4.8° whereas the angle between ring B and the thiophene ring C(5B) – S(9B) is 9.8°), although the C(4) – C(5) bond lengths (1.46(1) Å av.) (Table 1) suggest charge density delocalization on the whole ligand.

The asymmetric unit of complex **e**-DMSO contains two independent compound molecules, each one bearing a solvent molecule coordinated to the metal center, and two disordered free solvent molecules. In analogy to complexes **b** and **f**, the two rings formed by complexation of the metal atom by the 1,3-carbonyl ligands are almost planar (mean deviations from planarity are 0.069 for ring A(V1), 0.0196 for ring B(V1), 0.0842 for ring D(V2) and 0.0402 for ring E(V2)) and the 1,3-carbonyl units are bent towards the bound DMSO (the angles between the V(1) – O(1) and rings A and B are 94.4° and 101.9°, respectively and

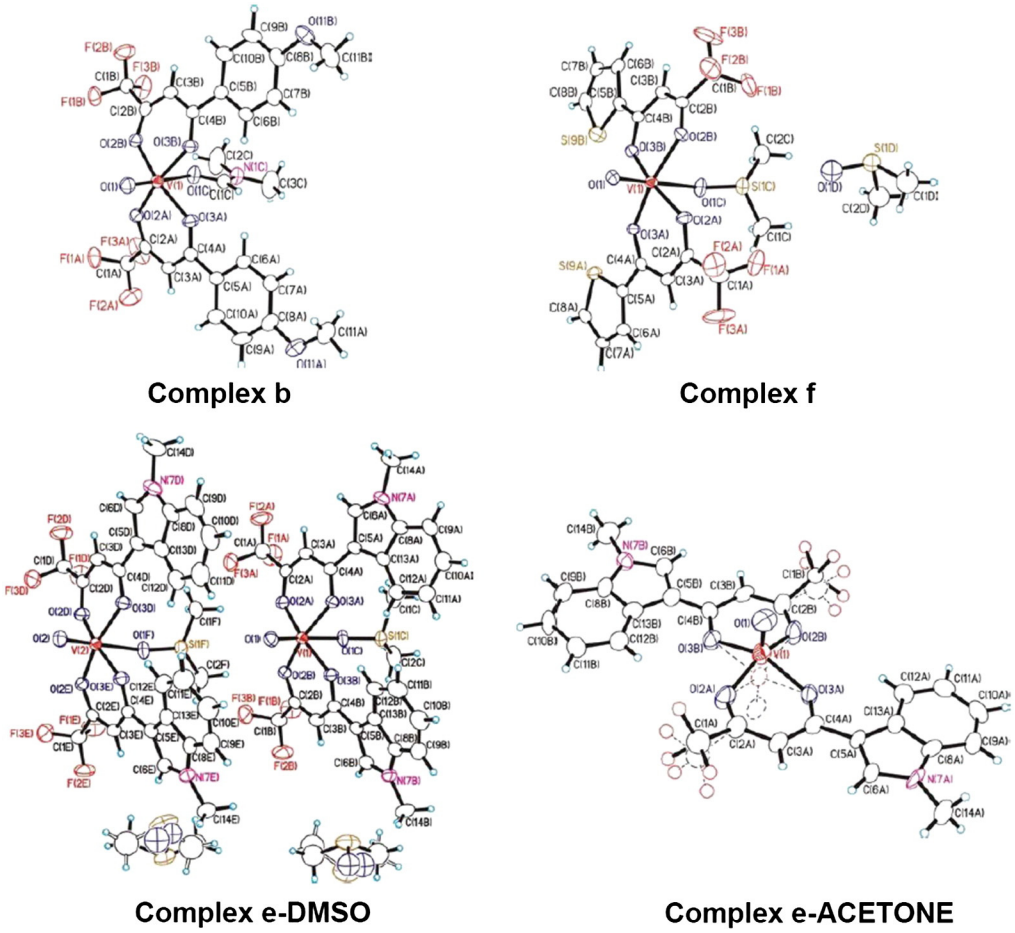


**Fig. 3.** Asymmetric unit content for complexes b, f, e-DMSO and e-ACETONE with atom labeling. Displacement ellipsoids for all but hydrogen atoms are drawn at 50% probability.

the angles between the V(2) – O(2) and the rings D and E are 91.3° and 107.5°, respectively). The great difference in these angles found within a same molecule suggests that ligands bending towards DMSO is due to the combined influence of electronic effects of the vanadyl oxygen and crystal packing. As in previous complexes, a deviation from planarity of the carbonyl ligands is evident in complex **e**-DMSO. This is due to the slight rotation of the indole moieties with respect to the 1,3-carbonyl planes (the angle between ring A and the indole moiety C(5A) – C(13A) is 5.7°, whereas the angle between ring B and the indole moiety C(5B) – C(13B) is 9.8°). In analogy to complexes **b** and **f**, the C(4) – C(5) bond lengths (1.433(5) Å av.) suggest charge density delocalization on the whole ligands. Due to the *cis*-planar arrangement, the two indole moieties are very close as the distances between the closest H atoms of the phenyl rings range between 2.41 and 2.64 Å: this suggests that steric interactions between the two indole moieties concur to their rotation, together with crystal packing.

As compared to the previous complexes, the species **e**-ACETONE represents an exception as it exhibits a square pyramidal geometry and does not coordinate the solvent. As in previous cases, both ligands lie in the equatorial plane, but their relative orientation is typical of a *trans*-planar isomer. The asymmetric unit contains one independent molecule of compound and the structure shows a great crystallographic disorder: the vanadyl group occupies two opposite positions with respect to the equatorial plane defined by the 1,3-carbonyl units, with distinct refined occupation factors of 79% and 21%. The $CF_3$ group of each carbonyl ligand lies as well in two distinct positions, with different refined occupation factors (65% and 35% for $CF_3$(A) and 58% and 42% for $CF_3$(B)). The 1,3-carbonyl units are bent downwards with respect to the vanadyl oxygen (the angles between the V(1) – O(1) and rings A and B are 96.2° and 93.1°, respectively and the angles between the V(1A) – O(1A) and the rings A and B are 96.6° and 93.3°, respectively). The agreement of these values with those found in complexes **b** and **e**-DMSO, whose metal center is six-coordinated, leads to the conclusion that solvent coordination does not influence the square pyramidal geometry of the $VO(O_4)$ moiety. This is also supported by the similar bond lengths found in **e**-DMSO and **e**-ACETONE. In contrast to complex **e**-DMSO, the indole moieties of **e**-ACETONE are almost coplanar with the 1,3-carbonyl planes (the angle between ring A and the indole moiety C(5A) – C(13A) is 2.4°, whereas the angle between ring B and the indole moiety C(5B) – C(13B) is 2.0°), due probably to the *trans*-planar arrangement of the ligands that minimize the steric interaction between the indole rings. The extended structural disorder prevents a more detailed molecular description of complex **e**-ACETONE.

Table 1 reports some relevant bond lengths and angles for complexes **b**, **f**, **e**-DMSO and **e**-ACETONE. Taking into account the e.s.d's of the reported bond distances, no significant differences on the V – O(1) bonds are found between the complexes. As far as the 1,3-carbonyl ligands is concerned, no significant differences are evident between the C(2) – O(2) and C(4) – O(3) bonds. V – O(2) bond distances in complex **b** are slightly longer than V – O(3), whereas they are similar in complex **f**; an inverted trend is found in complexes **e**-DMSO and **e**-ACETONE. As for the C(4) – C(5) bonds, they follow this trend: **b** > **f** > **e**. This can likely be related with the electronic properties of the substituents on the 1,3-carbonyl units: the higher electron-donor character of the indole moiety in complex **e** is responsible for the shorter C(4) – C(5) lengths and the longer V – O(3) bond. A comparison with complex [$Sc(CF_3COCHCOCH_3)_3$] that bears a non-electron donor methyl substituent on the β-dicarbonyl ligand [29] supports this statement (Table 1). As expected, the C(4) – C(5) length in the Sc(III) complex is longer as compared to complexes **b**, **f**, and **e**, whereas the

**Table 1**
Selected bond distances (Å) of the 1,3-carbonyl units from X-ray data for complexes **b**, **f**, **e**-DMSO, **e**-ACETONE and Sc(III)$(acac)_3$ and from DFT calculations for complexes **a**–**f** and $VO(acac)_2$.

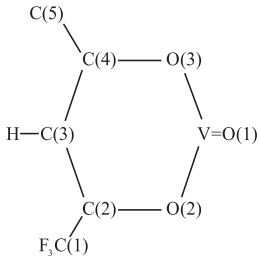


| Complex | Bond lengths | | | | | | | | | |
|---|---|---|---|---|---|---|---|---|---|---|
| | V–O(1) | V–O(2) | V–O(3) | C(2)–O(2) | C(4)–O(3) | C(1)–C(2) | C(2)–C(3) | C(3)–C(4) | C(4)–C(5) | V–$O_{solv}$ |
| *X-ray diffraction data* | | | | | | | | | | |
| **b** | 1.596(2) | 2.005(2) | 1.998(2) | 1.274(4) | 1.263(3) | 1.520(4) | 1.375(4) | 1.426(4) | 1.478(4) | 2.204(2) |
| | | 2.006(2) | 1.997(2) | 1.270(4) | 1.268(3) | 1.531(4) | 1.372(4) | 1.424(4) | 1.478(4) | |
| **f** | 1.603(5) | 2.008(5) | 2.010(5) | 1.268(9) | 1.276(9) | 1.53(1) | 1.37(1) | 1.40(1) | 1.46(1) | 2.174(5) |
| | | 2.021(5) | 2.015(5) | 1.267(9) | 1.274(8) | 1.52(1) | 1.36(1) | 1.41(1) | 1.46(1) | |
| **e**-DMSO | 1.598(3) | 1.998(2) | 2.011(2) | 1.293(4) | 1.283(4) | 1.524(5) | 1.348(5) | 1.422(5) | 1.431(5) | 2.190(3) |
| | | 1.993(2) | 2.007(2) | 1.287(4) | 1.272(4) | 1.520(5) | 1.351(5) | 1.433(5) | 1.429(5) | |
| | 1.600(3) | 1.996(2) | 2.022(2) | 1.283(4) | 1.279(4) | 1.519(5) | 1.358(5) | 1.431(5) | 1.432(5) | 2.190(3) |
| | | 1.976(2) | 2.010(2) | 1.289(4) | 1.276(4) | 1.516(5) | 1.362(5) | 1.429(5) | 1.441(5) | |
| **e**-ACETONE | 1.56(2) | 1.909(9) | 2.024(9) | 1.31(1) | 1.278(9) | 1.50(2) | 1.37(1) | 1.42(1) | 1.43(1) | |
| | 1.58(1) | 1.901(9) | 1.996(9) | 1.288(9) | 1.278(9) | 1.52(2) | 1.38(1) | 1.41(1) | 1.42(1) | |
| | | 1.944(6) | 1.978(6) | | | | | | | |
| | | 1.946(6) | 1.986(6) | | | | | | | |
| $[Sc(CH_3COCHCOCF_3)_3]$ | | 2.072(2) | 2.089(2) | 1.277(3) | 1.260(3) | 1.529(3) | 1.373(3) | 1.413(3) | 1.503(3) | |
| [29] | | 2.080(2) | 2.091(2) | 1.275(3) | 1.257(3) | 1.535(3) | 1.370(3) | 1.414(3) | 1.498(3) | |
| *DFT calculation results* | | | | | | | | | | |
| **a** | 1.559 | 1.991 | 1.998 | 1.270 | 1.274 | 1.537 | 1.384 | 1.415 | 1.485 | |
| **b** | 1.560 | 1.990 | 1.997 | 1.271 | 1.276 | 1.537 | 1.382 | 1.418 | 1.476 | |
| **c** | 1.560 | 1.992 | 1.998 | 1.270 | 1.276 | 1.537 | 1.384 | 1.416 | 1.483 | |
| **d** | 1.560 | 1.990 | 1.994 | 1.271 | 1.276 | 1.537 | 1.383 | 1.417 | 1.479 | |
| **e** | 1.562 | 1.993 | 1.987 | 1.278 | 1.278 | 1.533 | 1.376 | 1.427 | 1.446 | |
| **e**-DMSO | 1.569 | 2.029 | 2.031 | 1.273 | 1.269 | 1.534 | 1.377 | 1.429 | 1.455 | 2.294 |
| **e**-ACETONE | 1.563 | 2.009 | 2.003 | 1.272 | 1.273 | 1.534 | 1.379 | 1.427 | 1.451 | 2.572 |
| **f** | 1.559 | 1.991 | 1.999 | 1.272 | 1.277 | 1.536 | 1.382 | 1.417 | 1.456 | |
| **f**-DMSO | 1.568 | 2.035 | 2.030 | 1.271 | 1.267 | 1.537 | 1.382 | 1.423 | 1.462 | 2.266 |
| $[VO(acac)_2]$ | 1.564 | 1.993 | 1.993 | 1.275 | 1.275 | 1.507 | 1.401 | 1.401 | 1.507 | |
| [31] | | | | | | | | | | |

V–O(2) and V–O(3) lengths are similar. Furthermore, in all complexes, the C(2)–C(3) bond lengths are shorter than the C(3)–C(4), by a same extent. As the effect is the same in all compounds, it cannot be related with the substituents on C(4). It is rather due to the $CF_3$ group, although it does not reflect on the C(1)–C(2) bond lengths that are all close to the typical C–C single bond distance.

Finally, the distance between the oxygen of the solvent molecule coordinated to the vanadium atom (V–$O_{solv}$, Table 1) is larger for DMF (complex **b**) than for DMSO (complexes **f** and **e**-DMSO) and this suggests a stronger coordination ability of the DMSO solvent with respect to DMF.

### 3.3. DFT calculations

Optimized structures of complexes **a**–**f** show geometrical parameters in reasonable agreement with those measured experimentally (Table 1).

The structures were optimized without constraints in the gas phase. The discrepancies between the calculated geometries and the experimental ones (determined in the crystalline state) can be easily explained by considering the absence of intermolecular interactions and crystal forces that make the gas-phase optimized structures more similar to those found in solution. This is supported by previous studies on vanadyl complexes in solution that show the good match between computed structures and geometries inferred from ENDOR measurements [30]. In all compounds, the $VO(O_4)$ moiety has a square pyramid geometry with an average O(1)–V–O angle of 106°, the same found in the crystalline $[VO(acac)_2]$ complex [31]. The angle between V–O and the mean plane formed by the OC–C–CO fragment is close to 100° in all complexes, with the only exception of complex **a** (103°). The six-atom rings defined by the ketone carbonyls are not planar; the angle between the dihedral planes O(2)–V–O(3) and O(2)–C(2)–C(3)–C(4)–O(3) is ~13° in all cases, a value very close to that found in $[VO(acac)_2]$ (12°). Modeling of complexes **e** and **f** with an axially coordinated DMSO molecule induces a deformation of the square-based pyramid that results in O(1)–V–O angles of 97° instead of 106° found in the unsolvated complexes; this value is consistent with an almost octahedral arrangement.

Unlike the X-ray diffraction data, an influence of solvent coordination is found on the vanadyl oxygen: solvent coordination weakens the V–O bond that is longer as compared to the unsolvated complex (1.569 Å in **e**-DMSO vs. 1.562 Å in **e**; 1.568 Å in **f**-DMSO vs. 1.559 Å in **f**); accordingly, the computed $\nu$(V–O) frequency is lowered (1096 $cm^{-1}$ vs. 1127 $cm^{-1}$, respectively). Acetone, which is a weakly coordinating solvent, induces smaller geometry variations with respect to the unsolvated complex: **e**-ACETONE exhibits O(1)–V–O angles of 101° and a slightly lengthened V–O(1) bond (1.562 Å in **e** vs. 1.563 Å in **e**-ACETONE). Distinct solvent coordination effects are also highlighted by the $O_{solvent}$–vanadium bond length: V–$O_{solv}$ distance in **e**-DMSO and **f**-DMSO is 2.294 Å and 2.266 Å respectively, whereas it is 2.572 Å in **e**-ACETONE. Comparison between *cis*- and *trans*-planar arrangements of β-dicarbonyl ligands in complex **e** highlights inter-ligand

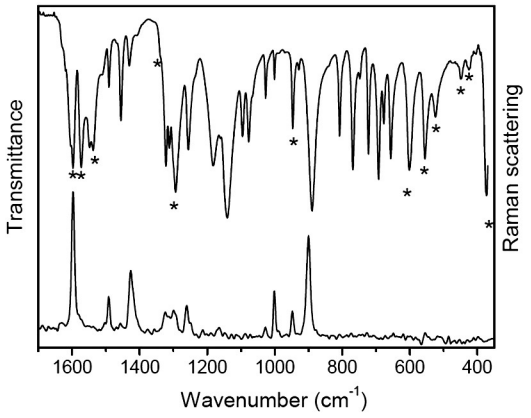


**Fig. 4.** Vibrational spectra (IR (top) and Raman (bottom)) of complex a. Asterisks indicate the modes of $(COCHCO)_2VO$ fragment.

**Table 3**
Absorption bands in the electronic spectra of complexes **a**–**f** in acetone, methanol and DMSO.

| Complex | Solvent | $\lambda_{max}$ (nm) | | | | | |
|---|---|---|---|---|---|---|---|
| **a** | Acetone | 743 | 606 | 470sh | | 357sh | |
| | MeOH | 756 | 605 | 481 | | 357sh | 336 |
| **b** | Acetone | 743 | 601 | 473sh | | 361sh | 346 |
| | MeOH | 756 | 603 | 480 | | 363sh | 350 |
| | DMSO | 779 | 620 | 487 | | 364sh | 350 |
| **c** | Acetone | 736 | 600w | 495sh | 443sh | 367sh | 343 |
| | MeOH | 751 | n.d. | 487sh | 444sh | 369sh | 347 |
| **d** | Acetone | 736 | 606w | 495sh | | 376 | |
| **e** | Acetone | 736 | 590w | 480sh | | 382 | 368 |
| | MeOH | 737 | 585 | n.d. | | 377 | |
| | DMSO | 790 | 625 | 488sh | | 375 | |
| **f** | Acetone | 744 | 605w | 496 | 416sh | 371sh | 350 |
| | MeOH | 756 | 602sh | 496 | 415sh | 371sh | 352 |
| | DMSO | 771 | 623 | 505 | 424sh | 374sh | 358 |

sh: shoulder; w: weak; n.d.: not detected.

steric effects: a *cis*-planar configuration induces a rotation of the aromatic moiety around the C(4)–C(5) bond (the angles between the aromatic plane and the β-dicarbonyl plane are 12° for the *cis*-planar complex and 5° for the *trans*-planar one), in agreement with the trend observed in the X-ray structures. This confirms the influence of steric effects over the geometry of these complexes that can be modified by crystal packing. This also explains the geometrical discrepancies between the solid-state structures and the structures computed in the gas phase.

Tiny differences are observed between the two C–O and V–O bonds of the β-dicarbonyl ligands, unlike shown by X-ray data. A more significant variation of the C–C lengths within the six-atom ring is found, both in the free and the coordinated ligand: the mean length of the C(3)–C(4) bond conjugated to the aromatic fragment is 1.417 Å, whereas the C(2)–C(3) bond adjacent to the $CF_3$ group is 1.383 Å long, in good agreement with the data collected in the solid state. This difference is explained by the electron-withdrawing effect of the $CF_3$ group that shifts electron density from the C–C bond of the enolic form of the ligand toward the C(1)–C(2) simple bond [32].

### 3.4. IR and Raman spectroscopies

Infrared and Raman spectra were recorded from samples synthesized and crystallized from ethanol solutions, a weakly coordinating solvent, so to minimize the possibility of hexa-coordinated vanadium center. The vibrational spectra of complexes **a**–**f** can be interpreted as derived from the contributions of three molecular fragments: the dicarbonyl $(COCHCO)_2VO$ unit, the $CF_3$ group and the aromatic moieties. Spectral assignments were done by comparing the spectral patterns of the complexes and the free ligands, and were based on previous assignments of vibrational spectra of vanadyl acetylacetonate complexes [33–35]. Assignments were checked through DFT computational calculations. A comparison of the vibrational patterns of complexes **a**–**f** with the uncoordinated ligands highlights that metal coordination does not affect significantly the principal internal modes of the $CF_3$ and R fragments; consequently, we focused mainly on the $(COCHCO)_2VO$ vibrations that usually are well detectable in the spectra (Fig. 4). Table 2 reports the most relevant vibrational modes. An inspection of the frequencies shows the close similarity of the vibrational pattern of the $(COCHCO)_2VO$ unit in complexes **a**–**f** as compared to $[VO(acac)_2]$ [36,37]: this suggests that complexes **a**–**f** share a square-pyramidal geometry and a similar force-field for the C–O, C–C and V–O bonds. The carbonyl modes are substantially similar in all complexes, too; this supports the presence of analogous coupling effects between the distinct aromatic moieties and the COCHCO vibrational modes. The $\nu_s$(C–O) mode in complexes **a**–**f** falls at higher frequency as compared to $[VO(acac)_2]$; the C–O bond length in complexes **a**–**f** is shorter, on average. The V═O stretching mode falls at 930–940 $cm^{-1}$, much lower than in crystalline $[VO(acac)_2]$. The dependence of this vibrational mode on the effects of neighboring species is well known [37]. The few samples recorded in $CCl_4$ solution (complexes **a** and **c**, as the other are insoluble in this solvent) do not show any variation of the $\nu$(V═O) stretching as compared to the solid state. Well-reproducible spectra of **e**-DMSO (to be compared with **e**) could not been recorded, probably due to the strong interaction of DMSO with the vanadyl ion that leads to the formation of differing species: this makes doubtful the assignment of the V═O stretching.

**Table 2**
IR and Raman absorptions of complexes **a**–**f**. The vibrational modes diagnostic of vanadyl coordination are reported.

| | $[VO(acac)_2]$ | Complex a | | Complex b | | Complex c | | Complex d | | Complex e | | Complex f | |
|---|---|---|---|---|---|---|---|---|---|---|---|---|---|
| | IR | IR | Raman | IR | Raman | IR | Raman | IR | Raman | IR | Raman | IR | Raman |
| $\nu_s$(C–O) | 1558s | 1597vs | | 1597s | | 1589vs | 1569w | 1596vs | | 1589s | | 1597s | |
| | | 1572vs | | 1576vs | | 1569s | | 1572s | | 1576s | | 1574vs | |
| $\nu_{as}$(C–C) | 1530vs | 1548s | | 1543vs | 1543w | 1535s | | 1535s | 1535vw | 1544s | | 1543vs | |
| | | 1538s | | | | | | | | 1538s | | | |
| $\nu_{as}$(C–O) | 1358s | 1338sh | | 1352s | | 1356m | 1356m | 1341m | 1341m | | | 1352s | 1352m |
| $\nu_s$(C–C) | 1287m-s | 1293vs | 1293m | 1297s-sh | 1297m | 1292vvs | 1292m | 1292vvs | | 1278vs | 1280w | 1295s | 1295vw |
| $\nu$(V═O) | 998s | 947s | 947m | 939m-s | 942s | 938m | 938m-w | 945m | 940m(sh) | 930(sh) | 930m | 939s | 939m |
| | 610m-w | 601s | | 598s | | 597s | | 600s | | 604s | | 597s | |
| | 561vvw | 556s | | 550 | | 527 | | 530 | | 569 | | 551 | |
| $\nu$(V–O) | 483s | 524m | | 525 | | 517 | | 523 | | 531s | | 527 | |
| | 463m | 448w | | 458 | | 448 | | | | | | | |
| | 424m | 424w | | 414 | | 424 | | | | 408 | | 416 | |
| $\delta_{O-V-O}$ | 366m | 373s | | 352s | | 356s | | 363s | | 360s | | 374s | |

### 3.5. Optical spectra

Table 3 reports the $\lambda_{max}$ of the electronic spectra of complexes **a**–**f** in three different solvents.

All spectra were characterized by three bands in the 800–400 nm range, with the exception of complexes **c** and **f** that exhibited a fourth absorption around 443 nm and 416 respectively.

Depending on the solvent, the $[VO(acac)_2]$ absorptions reported in the literature [38–40] fall respectively around 750–780 nm, 580–600 nm and 390–400 nm and the three bands are assignable to the following transitions: $b_2 \rightarrow e_\pi^*$ (band I); $b_2 \rightarrow b_1^*$ (band II) and $b_2 \rightarrow a_1^*$ (band III) according to the MO scheme proposed by Ballhausen [39]. These data are in substantial agreement with our experimental findings on complexes **a**–**f**, although assignments are complicated by the contribution of ligands' chromophores to the spectra, as well as by the presence of vanadyl charge-transfer bands that may overlap to band III. Due to this fact, band III is often detected as a shoulder of absorption bands at lower wavelength. In addition, the band position is affected by the polarity and the coordination ability of the solvent. In fact, replacement of acetone with methanol brought about a slight blue-shift of band I for all complexes **a**–**f**. The shift was more evident in the presence of DMSO, a strongly coordinating solvent. Band II was almost insensitive to solvents and fell around 600 nm in all conditions, except in the presence of DMSO that shifted the absorption at λ ~620 nm. A red-shift effect by DMSO was also noticed on the band at λ ~485 nm.

Complexes **c** and **f** exhibited a fourth absorption band above 400 nm. According to Garribba et al. [19,41] this might arise from symmetry distortions, although the superposition of contributions from the ligands and the vanadyl moiety in this spectral region make the interpretation of these data not straightforward. Slight differences in the position of band at λ < 400 nm in the electronic spectra of complexes **a**–**b** and **c**–**d** were likely due to the inductive effect of the methoxyl substituent on the aromatic ring. Assignment of these bands to the ligands is justified by their invariance upon solvent change.

The solubility of all complexes was higher in acetone as compared to methanol.

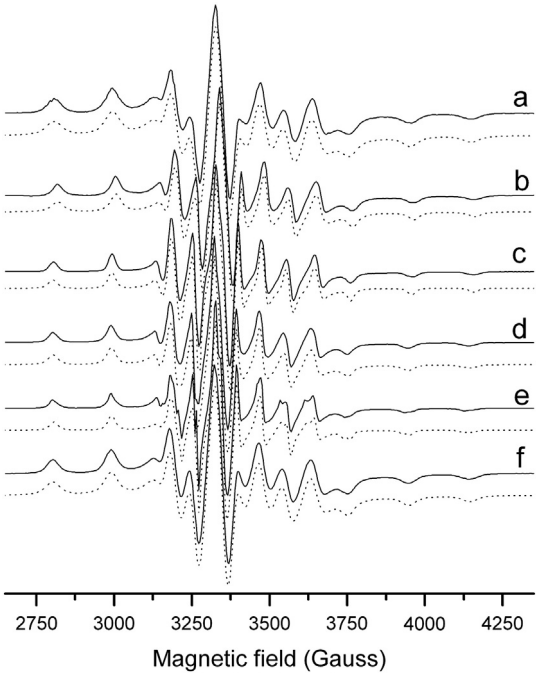


**Fig. 5.** A and B — 77 K EPR spectra of complexes **a**–**f** dissolved in acetone.

**Table 4**
EPR parameters for vanadyl complexes **a**–**f** in acetone at 77 K. The spin Hamiltonian parameters were determined by spectral simulation carried out with the Sim32 software [26].

| Complex | Solvent | Spectral contribution (%) | g⊥ | g∥ | A⊥ ($cm^{-1}\cdot10^4$) | A∥ ($cm^{-1}\cdot10^4$) |
|---|---|---|---|---|---|---|
| **a** | Acetone | 100 | 1.9821 | 1.9429 | 64.81 | 173.7 |
| **b** | Acetone | 100 | 1.9815 | 1.9419 | 64.99 | 173.7 |
| | DMSO | 100 | 1.9811 | 1.9452 | 63.49 | 171.5 |
| **c** | Acetone | 100 | 1.9818 | 1.9434 | 64.4 | 172.6 |
| **d** | Acetone | 58.6 | 1.9806 | 1.9467 | 62.14 | 170.2 |
| | | 41.4 | 1.9827 | 1.9411 | 66.46 | 174.3 |
| **e** | Acetone | 44.5 | 1.9826 | 1.9482 | 60.5 | 170.6 |
| | | 55.5 | 1.9817 | 1.9385 | 66.1 | 173.7 |
| | DMSO | 100 | 1.9793 | 1.9434 | 62.78 | 171.4 |
| **f** | Acetone | 100 | 1.9815 | 1.9428 | 64.6 | 173.9 |
| | DMSO | 100 | 1.9852 | 1.9406 | 66.52 | – |

### 3.6. Complex stability in solution assessed by NMR and optical spectroscopy

The complex stability in solution was assessed by $^1$H NMR and optical spectroscopy.

$^1$H NMR spectra of complexes **a**–**d** were recorded in $d^4$-methanol, $d^6$-acetone and $d^6$-DMSO after 5-day, 2-week and 4-week incubation at RT. Based on the invariance of the $^1$H NMR pattern vs. time, complex **c** dissolved in acetone or DMSO was found stable over the full time range and over the 20–80 °C temperature range. Conversely, methanol affected its stability, as a 5-day incubation at RT resulted in the appearance of $^1$H NMR signals assignable to the free ligand (Fig. 2, middle trace). This might be related with the lower coordination strength of methanol as compared to the other two solvents. The other complexes exhibited a similar behavior: a rough quantitative analysis of NMR data shows that the vanadyl complexes in methanol solution exhibit the following stability order: **a**, **b** < **d** < **c**.

In agreement with the $^1$H NMR evidence, the optical spectrum of complex **c** in acetone did not highlight changes even after 26-day incubation at room temperature, whereas significant spectral changes were found in methanol after 5 days. Conversely, complex **a** was affected by both solvents, although by methanol to a higher extent. Optical data thus confirm the NMR experimental evidence.

### 3.7. EPR spectra

Fig. 5 reports the experimental and calculated EPR spectra of complexes **a**–**f** dissolved in acetone recorded at 77 K. Spectral simulations show that the spectral pattern of complexes **a**, **b**, **c**, and **f** stems from a single species whereas two distinct spectral contributions, assignable to distinct species, are found in complexes **d** and **e**. The spin Hamiltonian parameters reported in Table 4 suggest that the single species found in complexes **a**, **b**, **c**, and **f** coincides with one of the two species found in complexes **d** and **e**. Spectral parameters of complexes **b**, **e** and **f** dissolved in DMSO show that this solvent, which is reported to coordinate to the sixth vacant site of the vanadium center, lowers A as expected.

77 K EPR spectra of complexes **a**–**f** treated according to the protocol employed for biological tests (i.e. dissolved in a small volume of DMSO and diluted with the biological medium employed for cell tests) are similar to those recorded in DMSO and have not been reported.

### 3.8. Cell tests

The effect of complexes **a**–**f** on the viability of two non-tumor cell lines, hTERT-HME1 and podocytes, and two colorectal cancer cell lines, HCT 116 and HT-29, was evaluated. Complexes **a**–**f** inhibited hTERT-HME1 viability in a dose-dependent manner (Fig. 6A): the effect of complexes **a**–**d** and **f** was similar to that induced by $VOSO_4$.

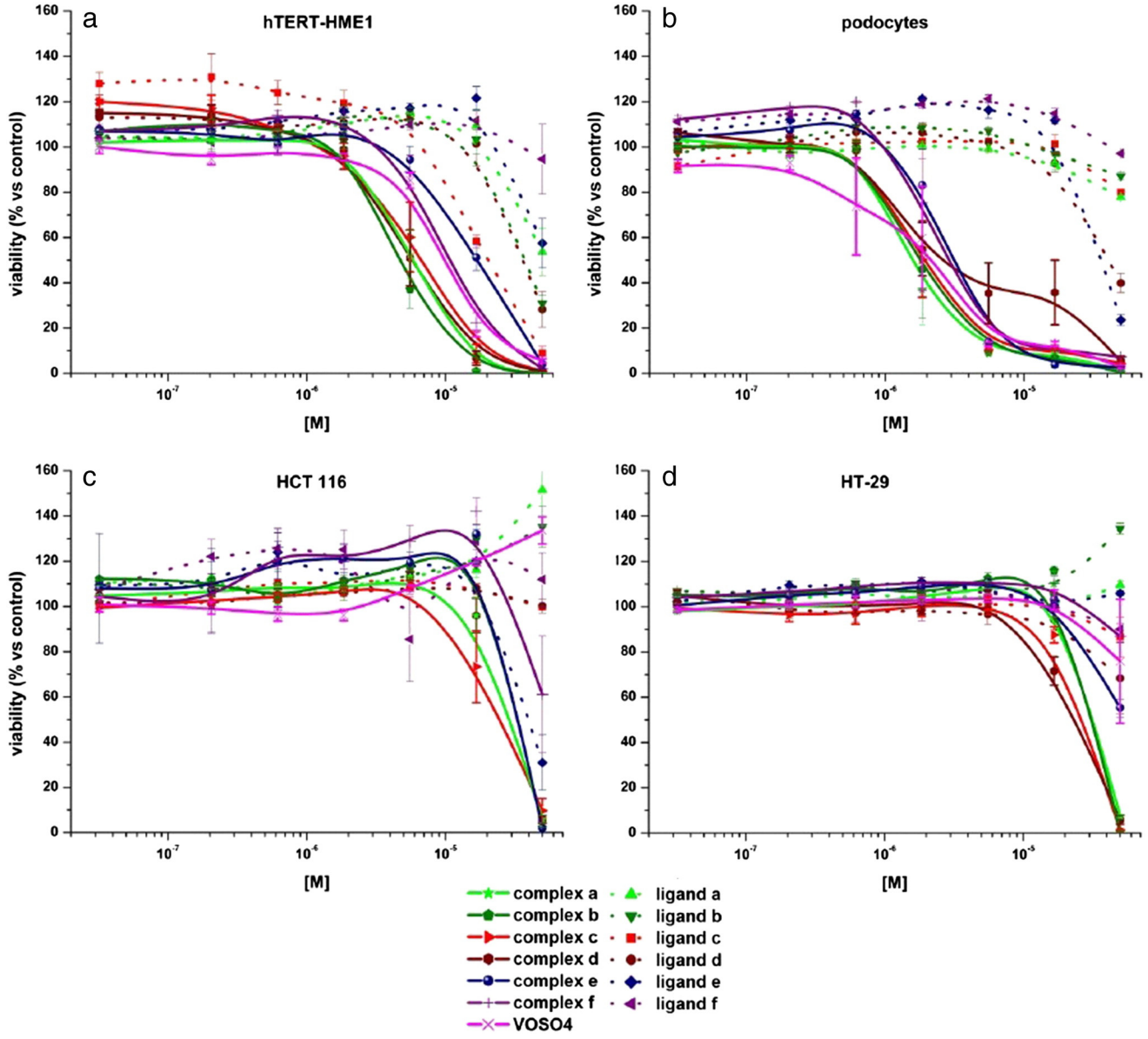


**Fig. 6.** Effect of complexes a–f on cell viability. Each cell line was treated with complexes a–f, $VOSO_4$ and the respective ligands. Cell viability was estimated by determining ATP content in three replicate wells. Results are normalized to the growth of cells treated with DMSO and are represented as mean ± SEM of at least three independent experiments.

Conversely complex **e** exhibited an $IC_{50}$ significantly greater as compared to $VOSO_4$ (17.40 ± 10.18 vs 9.85 ± 1.20, respectively; Table 5). All ligands, but ligand **f**, influenced cell viability although their effect was significantly lower as compared to the corresponding complex. The inhibition of podocyte viability by complexes **a**–**f** was dose-dependent (Fig. 6B); a similar result was found in the presence of $VOSO_4$: $IC_{50}$ values reported in Table 5 highlight that the behavior of the complexes was not statistically different from $VOSO_4$. Once again, the ligands alone (in particular ligands **e** and **f**) affected cell viability, although their $IC_{50}$ values were almost one order of magnitude lower as compared to the corresponding compounds.

Colocancer cell lines provided a distinct response to complexes **a**–**f**. Both cell lines were insensitive to $VOSO_4$. Complexes **a**–**d** at the highest concentration (50 μM) completely inhibited HCT 116 viability, whereas their respective ligands were inactive (Fig. 6C; Table 5). Complex **e** was as effective as ligand **e**, whereas complex **f** was able to inhibit cell proliferation by a 40% factor. Ligand **f** was ineffective. HT-29 cells were more sensitive to complexes **a**–**d** as compared to complexes **e** and **f**. In fact, complex **e** exhibited only a 40% of viability inhibition. The ligands were completely ineffective (Fig. 6D; Table 5).

In summary, complexes **a**–**f** affected the viability of all the tested cell lines to a different extent. Non-tumor cell lines were more sensitive than tumor cell lines, and podocytes turned out to be the most sensitive cell line (Fig. 6 and supplementary Fig. 12S). Interestingly, $VOSO_4$ uniquely affected normal cells and was ineffective towards tumor cell lines (supplementary Fig. 12S).

**Table 5**
IC50 values for vanadyl complexes **a**–**f** tested on 4 distinct cell lines.

| Complex | IC50 (mM)[a] | | | |
|---|---|---|---|---|
| | hTERT-HME1 | Podocytes | HCT 116 | HT-29 |
| **a** | 5.83 ± 1.21 | 1.53 ± 1.23 | 29.23 ± 3.28[b] | 31.70 ± 3.28[b] |
| **b** | 4.74 ± 1.21 | 1.82 ± 1.26 | 32.90 ± 2.97[b] | 31.00 ± 3.28[b] |
| **c** | 6.68 ± 1.26 | 1.97 ± 1.24 | 24.39 ± 4.28[b] | 26.03 ± 1.75[b] |
| **d** | 5.64 ± 1.20 | 2.51 ± 1.29 | 28.70 ± 2.30[b] | 23.10 ± 1.20[b] |
| **e** | 17.40 ± 1.20 b | 2.98 ± 1.29 | 33.40 ± 3.30[b] | >50.00 |
| **f** | 11.04 ± 1.30 | 3.13 ± 1.38 | >50.00 | >50.00 |
| $VOSO_4$ | 9.85 ± 1.20 | 2.12 ± 1.35 | >50.00 | >50.00 |

[a] Values are means ± SE; n ≥ 3.
[b] $P < 0.05$ versus $VOSO_4$.

## 4. Discussion

Complexes **a**–**f** are characterized by ligands with increasing steric hindrance and distinct electron density distributions. The latter is modulated by the presence or absence of a methoxyl moiety or of electron-rich heteroaromatic rings.

Complexation of the vanadyl moiety by ligands **a**–**f** is demonstrated by ESI-MS and NMR experimental findings. ESI data show that, in all cases, a 2:1 ligand:vanadyl ratio is found, although partial disruption of the complex may occur within the ionization chamber of the ESI instrument.

The characterization of the newly synthesized complexes was carried out both in the solid state and in solution.

Complexes **a**–**f** in the solid state were investigated by X-ray diffraction, IR and Raman spectroscopy and the assignments were supported by DFT calculations.

The solution state of complexes **a**–**f** was characterized by UV–Vis and EPR spectroscopies.

A comparison between the two states is important, as vanadyl complexes are known to undergo speciation equilibria that are strongly dependent on the solvent, the pH and the ligands. These processes may include solvent coordination and isomerization [19,20] and may influence the pharmacological potential of the species.

### 4.1. Characterization of complexes a–f in the solid state

Both crystallographic and vibrational data show that, in the solid state, complexes **a**–**f** exist either in square pyramidal or in the distorted octahedral geometry, with the two acac-derived ligands lying in the equatorial plane and thus defining a *trans* isomer with respect to the 6th coordination site [42]. The square-planar geometry was found when crystals were separated from non-coordinating or weakly-coordinating solvents, such as ethanol or acetone, whereas the distorted octahedral geometry was typical of crystals separated from stronger coordinating solvents such as DMF or DMSO. In fact, the V═O stretching frequencies recorded on complexes crystallized from ethanol suggest assignments to non-solvent-coordinated species.

This is clearly highlighted by the X-ray structures of complex **e**, crystallized from acetone or DMSO, and **f**, crystallized from DMSO. Based on the crystallographic structure, DMSO coordinates the vanadium center through the oxygen atom of the sulfoxide moiety and it occupies the 6th coordination position that is vacant. This arrangement was confirmed by DFT calculations on complex **f** and agrees with the structure of other vanadyl complexes reported in the literature [19]. Conversely, the 6th axial coordination site in complex **e**-ACETONE is free.

As ligands **a**–**f** bear asymmetric substitutions on the β-dicarbonyl moiety, an additional *cis*/*trans* isomerism was possible *in the plane*. Two isomers could form, either with the $CF_3$ group of each ligand in *cis*-planar or *trans*-planar arrangements with respect to each other. Crystallographic data on 4 complexes show that the *cis*-planar isomer is always found in the presence of strongly coordinating solvents, whereas complex **e** crystallized from acetone was a *trans*-planar isomer.

As the formation of the *cis*-planar isomer is generally unfavored for sterical reasons, a stabilization effect exerted by the solvent molecule coordinated to the metal center may be posited. As an alternative explanation, this experimental behavior might be related with polarity: the *cis*-planar and *trans*-planar isomers exhibit distinct dipolar momentum. Thus, a selective crystallization might have occurred, depending on the solvent.

Both crystallographic data and DFT calculation show that the pyramidal geometry defined by the $V(O)O_4$ moiety is distorted and the rings defined by the carbonyl units are bent towards the 6th coordination site, both in solvent-coordinated and uncoordinated complexes. Such distortion is likely due to the repulsion effect exerted by the vanadyl oxygen towards the donor oxygens of the carbonyl moiety, although some influence of the crystal packing has also to be invoked. It is unclear whether an influence of the coordinated solvent plays a role in the distortion, due to the disagreement between the X-ray and DFT-computed structures.

Both DFT calculations and X-ray data highlight the electron-withdrawing effect of the $CF_3$ moiety that results in shortened C(2)–C(3) bond lengths as compared to the C(3)–C(4) bond, within the 1,3-dicarbonyl unit. X-ray data also highlight a significant electronic influence of the aromatic substituent on the 1,3 carbonyl moiety that results in shortened C(4)–C(5) and longer V(1)–O(3) bond lengths: this is due to the stronger electron-donating character of the indole moiety (in complex **e**) as compared to the methoxyphenyl and the thiophene rings of complexes **b** and **f**, respectively.

A steric intermolecular interaction is also observed between the two more encumbering indole substituents in the *cis*-planar complexes that cause a slight deviation of planarity of the 1,3-carbonyl ligands.

Finally the interaction of DMSO with the vanadium center results in shorter $V-O_{solv}$ distances with respect to the complexes with other coordinated solvents or with the uncoordinated ones, in agreement with the stronger coordinating properties of the former. DFT calculations have also highlighted the trans-effect exerted by the solvent coordinated in the sixth position that reflects in an elongation of the V═O bond in the presence of the strongly coordinating solvent DMSO.

### 4.2. Characterization of complexes a–f in solution

A characterization of complexes **a**–**f** in solution was carried out by UV–Vis and EPR spectroscopy.

A comparison between the solid and the solution state is necessary, as vanadyl compounds are reported to undergo complex equilibria that may result in ligand replacements by solvent molecules, isomerization, establishment of labile or stable interactions between the metal complex and the solvent. These phenomena are strongly dependent on the kinetic and thermodynamic stability of the possible isomers, the coordinating properties of solvents, pH effects (when applicable), the ligand basicity, etc. Discriminating between isomers or mono- and bis-chelated complexes is relevant, as distinct molecular arrangements may affect the mode of interaction of vanadyl complexes with biological targets.

The optical spectra of vanadyl complexes may help to assign the coordination geometry in solution and to establish whether a solvent is coordinated or not to the vanadyl center, as they are sensitive to solvent polarity and coordination ability [19,38,40,41].

Optical spectra of vanadyl complexes show three bands associated with the vanadyl moiety. Band I (around 780 nm) is known to be sensitive to coordination changes along the $VO^{2+}$ axis. Garribba et al. [19,41] report that the coordination of a solvent molecule on the axial site results in a stabilization of the $e_\pi^*$ level and brings about a red-shift with respect to the square pyramidal complex. This criterion may help to discriminate between 5- and 6-coordinated vanadyl complexes. In addition, band I is strongly sensitive to symmetry: a trigonal distortion that drives the system from the $C_4v$ symmetry, typical of square pyramidal complexes, towards $C_2v$ symmetry splits the $e_\pi^*$ level [41], giving rise to two absorptions that may fall at $\lambda > 800$ nm and $\lambda < 600$ nm. Band II (around 580 nm) is relatively weak and is sensitive to equatorial contributions, as level $b_1^*$ derives from the contributions of $d_{x2-y2}$ orbitals of vanadium and orbitals from the ligands: it is almost unaffected by the solvent. Band III falls around 390 nm and it is often found as a shoulder, due to the superposition with the vanadyl charge-transfer bands or the absorptions from the ligands. According to Bernal [38], a slight influence of solvent coordination is expected on this absorption too, as level $a_1^*$ contains contributions from the $d_{z2}$ orbital of vanadium and from ligands; nevertheless, the solvent effect is a minor one, as compared to band I. In summary, the presence of 3 bands between 400 and 850 nm is taken as an evidence of $C_4v$ symmetry (square pyramidal complex) [19,41], whereas 4 absorptions suggest a trigonal distortion. Depending on the extent of distortion, a corresponding splitting of g values in the EPR spectra may be found [43].

Unambiguous spectral assignment of vanadyl bands may be done based on the relationship between the optical transition energy and the g values, as reported by Bernal [38]. According to this equation, the absorption at ~730–790 nm corresponds to g ~1.98 and is assignable to transition I; whereas the absorption at ~590–620 nm corresponds to g ~1.94 and is assignable to transition II. The latter assignment is supported by the negligible solvent-dependence expected for this transition. As band I of complexes **a**–**f** is not splitted and the EPR data are consistent with an axial rather than a rhombic symmetry, a $C_4v$ symmetry is predicted for all complexes **a**–**f** in acetone solution.

Assignments of bands between 500 and 430 nm is more difficult, as the absorption maxima do not correspond to those expected for band III. In fact, Rangel et al. [43] report that band III is often hidden by other absorptions, i.e. charge-transfer bands and absorption from the ligands.

Absorptions at $\lambda < 400$ nm are likely to arise mainly from the ligands: the almost coincidence of the absorption maxima in similar ligands (e.g. ligands **a** and **b**, or **c** and **d**) and the absence of solvent effects support this conclusion and rule out their assignment to transition III.

Finally, the marked red-shift of band I in complexes dissolved in DMSO suggests that a molecule of this strongly coordinating solvent enters the first coordination sphere of vanadium, in agreement with X-ray data available on complex **e**-DMSO. The increasing red-shift of band I with increasing coordination strength of the solvent (acetone < MeOH < DMSO) agrees with the expectations [19].

UV–Vis assignments rule out dramatic symmetry distortions towards the trigonal bipyramidal geometry that might be expected in 5-coordinated complexes.

The analysis of the EPR data at 77 K (in acetone and DMSO) shows spin-Hamiltonian parameters that are consistent with those reported in the literature for vanadyl complexes with acac-ligand derivatives [19]. Spectral simulation highlights that all complexes, but **d** and **e**, are characterized by a single species. Hyperfine coupling constant A and g values of complexes **a**, **b**, **c** and **f** correspond to those of species 2 in complexes **d** and **e**.

The literature data available on the equilibria undergone by the vanadyl systems in solution brings forth four distinct hypothesis with regard to these species: i) the presence of *cis*/*trans* isomerism in space; ii) the presence of a mixture of bis- and mono-chelate complexes; iii) the presence of *cis*/*trans* isomerism in the equatorial plane; and iv) the presence of solvent coordination equilibria.

Hypothesis i) is unlikely, as *cis*/*trans* isomers in space should result in rhombic spectral patterns [3,6,19,43–45] that are never associated to complexes **a**–**f**.

A comparison with a salicylaldehyde-derivative of vanadyl complexes reported by Costa-Pessoa [44] shows that the A and g values of complexes **a**–**f** might be consistent with the bis-chelate complex (species 2, higher A value) and the mono-chelate complex (species 1, lower A value). According to this assignment, complexes **a**, **b**, **c** and **f** would be the bis-chelated form, whereas the mono-chelated form would exists only for complexes **d** and **e**, a hypothesis in agreement with the stability data. As the EPR spectra are recorded in acetone, this would imply the coordination of at least two acetone molecules in the equatorial plane. Acetone is reported as a very weakly-coordinating solvent [42,46]; as a consequence, its coordination in equatorial position seems unlikely. Although, evidence reported by Costes [47] shows an acetone molecule coordinated to the vanadium center of a Gd-vanadyl complex. This assignment is also supported by decreased A values with increased in plane π-bonding in 1,3-butandionate complexes [44] that is reflected in the A values of species 1 vs. species 2 in complexes **d** and **e**. On the other hand, ENDOR studies on $[VO(acac)_2]$ in acetone [42,46] show that this solvent may, at the utmost, establish weak interactions with the vanadyl oxygen or the ligands. Most probably, the possibility for acetone to interact with the vanadium center is strongly dependent on the electron-acceptor properties of the metal center that are modulated by the electronic properties of ligands.

Hypothesis iii) has never been reported to result in meaningful changes of the A parameters and it is thus discarded. In fact, a *cis*/*trans* isomerism in the equatorial plane keeps the first coordination sphere of the metal unchanged: no changes of the coupling constant should be expected in this case, according to the additivity relationship [48,49].

Finally, species 1 and 2 in complexes **d** and **e** might arise from an equilibrium between the solvent-coordinated and non-coordinated complex on the axial coordination site. According to Gorelsky et al. [50] the presence of a solvent molecule in the axial position should consistently reduce A values, whereas A in species 1 is only slightly lower than in species 2. In addition, a comparison with the X-ray structure of complex **e**-ACETONE highlights the absence of solvent molecules coordinated to the metal center in such position. By analogy, the axial coordination of acetone seems unlikely to occur in the complex in solution and may be ruled out.

As a conclusion, the overall optical and EPR evidence suggests that complexes **a**–**f** are in $C_4v$ symmetry: the absence of rhombicity in the EPR spectra rules out dramatic symmetry distortions in the system. The analysis of the spin Hamiltonian parameters suggests that – according to similar complexes reported in the literature [19,42] – complexes **a**–**f** bear both ligands in the equatorial plane, although *cis*-planar and *trans*-planar isomers cannot be distinguished based on the spectral parameters. Conversely, the presence of mono-chelate complexes may be tentatively postulated for complexes **d** and **e**. A conclusive assignment of these species requires further investigations by ENDOR and pulsed EPR spectroscopy.

### 4.3. Cell tests

Tests on cell viability were carried out on non-tumor and tumor cells. Two colon cancer cell lines were selected as they are known to be sensitive to platinum-based chemotherapy (e.g., FOLFOX that contains oxaliplatin) and, by extension, are expected to respond to other metal complexes, namely vanadyl compounds.

Our experimental findings showed that normal cell lines are more sensitive to complexes **a**–**f** as compared to tumor cells. They are also responsive to vanadyl sulphate: this suggests that the effect of complexes is mainly due to the vanadyl moiety and the influence of the ligands is negligible in the case of non-tumor cells.

Interestingly, tumor cell lines are sensitive to complexes **a**–**f** but resistant to vanadyl sulphate as well as to ligands. A specific effect related with the whole complex, and not solely to the vanadyl moiety, may thus be speculated. Ligands undoubtedly play a modulating role, as the experimental data show that cells are less responsive to complexes **e** and **f** as compared to the other vanadyl compounds.

In fact, the possibility of fine-tuning the effects of vanadium (minimizing adverse effects and preserving the benefits) by modulating the structure of organic ligands is demonstrated by a number of studies on insulin-mimetic vanadium complexes [51]. The ligands may influence the absorption, tissue uptake and intracellular mobility of vanadium. More specifically, they are crucial in determining the ability of a complex to cross biological membranes, a requirement that is mostly important for those metals whose absorption relies on passive diffusion, such is the case of vanadium. A good balance between lipophilicity and hydrophilicity of the complexes is crucial in modulating the uptake. The responsiveness of tumor cells to complexes **a**–**f** as compared to the $VO^{2+}$ ion might be explained in the light of these considerations. Further, the distinct response to complexes by the two tumor cell lines is not unexpected, as these lines display different histological origin and, consequently, different protein and enzyme expression. Typically, HT-29 cells derived from a colorectal adenocarcinoma show a basal overexpression of COX-2, whereas HCT116 cells (isolated from a patient with a colorectal carcinoma) do not express COX-2 constitutively.

The experimental data suggest that the effectiveness of complexes **a**–**f** on tumor cell lines may be improved by modulating the ligand structure, in order to get compounds that are selectively active towards

tumor cells and ineffective or little effective towards non-tumor cell lines.

These very preliminary data highlight the need for a thorough study of the mechanism that lies behind the distinct response of the selected cell lines to complexes and the $VO^{2+}$ ion.

## 5. Conclusions

In summary, vanadyl complexes **a**–**f** have been synthesized and characterized in the solid state as well as in solution. According to previous results on vanadyl complexes with acac-derivatives, compounds **a**–**f** display a square pyramidal geometry with two ligands in the equatorial plane. In the presence of strongly coordinating solvents, *cis*-planar isomers seem to be favored.

All complexes exhibit a good stability in solution, although EPR data suggest the presence of both the bis- and the mono-chelate forms of complexes **d** and **e**. Further investigation is needed to confirm this assignment.

Preliminary test of complexes **a**–**f** on normal and tumor cells shows that these complexes are effective in inhibiting cell viability. In normal cell, this effect seems mainly related with the vanadyl moiety, whereas the responsiveness of tumor cells seems to be mediated by the ligands' properties.

Further investigations are needed to clarify this point and consequently improve the complex selectivity towards tumor cells.

*Abbreviations*

| | |
|---|---|
| COX-2 | cyclooxygenase 2 |
| DMF | dimethylformamide |
| DFT | density functional theory |
| EI | Electronic Impact |
| ESI-MS | Electron Spray Ionization Mass Spectrometry |
| e.s.d. | estimated standard deviation |

## Appendix A. Supplementary data

Supplementary data to this article can be found online at http://dx.doi.org/10.1016/j.jinorgbio.2013.07.015.

## References


[1] R.K.B. Devi, S.P. Devi, R.K.H. Singh, Spectrosc. Lett. 45 (2012) 93–103.
[2] J. Korbecki, I. Baranowska-Bosiacka, I. Gutowska, D. Chlubek, Acta Biochim. Pol. 59 (2012) 195–200.
[3] E.G. Ferrer, M.V. Salinas, M.J. Correa, L. Naso, D.A. Barrio, S.B. Etcheverry, L. Lezama, T. Rojo, P.A.M. Williams, Biol. Inorg. Chem. 11 (2006) 791–801.
[4] M.S. Molinuevo, A.M. Cortizo, S.B. Etcheverry, Cancer Chemother. Pharmacol. 61 (2008) 767–773.
[5] A.M. Evangelou, Crit. Rev. Oncol. Hematol. 42 (2002) 249–265.
[6] J. Benítez, L. Guggeri, I. Tomaz, J. Costa Pessoa, V. Moreno, J. Lorenzo, F.X. Avilés, B. Garat, D. Gambino, J. Inorg. Biochem. 103 (2009) 1386–1394.
[7] G.T. Morgan, H.W. Moss, J. Chem. Soc. 103 (1914) 78.
[8] D.C. Crans, J. Inorg. Biochem. 80 (2000) 123–131.
[9] N. Butenko, A.I. Tomaz, O. Nouri, E. Escribano, V. Moreno, S. Gama, V. Ribeiro, J. Paulo Telo, J. Costa Pessoa, I. Cavaco, J. Inorg. Biochem. 103 (2009) 622–632.
[10] Y. Fu, Q. Wang, X.-G. Yang, X.-D. Yang, K. Wang, J. Biol. Inorg. Chem. 13 (2008) 1001–1009.
[11] J. Li, G. Elberg, D.C. Crans, Y. Shechter, Biochemistry 35 (1996) 8314–8318.
[12] K.H. Thompson, C. Orvig, Coord. Chem. Rev. 219–221 (2001) 1033–1053.
[13] Y. Zhao, J. Ye, H. Liu, Q. Xia, Y. Zhang, X. Yang, K. Wang, J. Inorg. Biochem. 104 (2010) 371–378.
[14] D. Mustafi, B. Peng, S. Foxley, M. Makinen, G. Karczmar, M. Zamora, J. Ejnik, H. Martin, J. Biol. Inorg. Chem. 14 (2009) 1187–1197.
[15] S.S. Amin, K. Cryer, B. Zhang, S.K. Dutta, S.S. Eaton, O.P. Anderson, S.M. Miller, B.A. Reul, S.M. Brichard, D.C. Crans, Inorg. Chem. 39 (2000) 406–416.
[16] B.P. Baranwal, K. Tripathi, A.K. Singh, S. Tripathi, Spectrochim. Acta A 91 (2012) 365–369.
[17] K.H. Thompson, K. Bohmerle, E. Polishchuk, C. Martins, P. Toleikis, J. Tse, V. Yuen, J.H. McNeill, C. Orvig, J. Inorg. Biochem. 98 (2004) 2063–2070.
[18] P.-K. Hon, R.L. Belford, C.E. Pfluger, J. Chem. Phys. 43 (1965) 1323–1333.
[19] E. Garribba, G. Micera, D. Sanna, Inorg. Chim. Acta 359 (2006) 4470–4476.
[20] G.R. Hanson, Y.S. Sun, C. Orvig, Inorg. Chem. 35 (1996) 6507–6512.
[21] B. Nagarajan, B. Muller, O. Storcheva, K. Kohler, A. Poppl, Res. Chem. Intermed. 33 (2007) 705–724.
[22] B. Kirste, H. van Willigen, J. Phys. Chem. 86 (1982) 2743–2749.
[23] Y. Li, Y. Zhao, J. Fluoresc. 19 (2009) 641–647.
[24] P. Diana, A. Carbone, P. Barraja, A. Montalbano, B. Parrino, A. Lopergolo, M. Pennati, N. Zaffaroni, G. Cirrincione, ChemMedChem 6 (2011) 1300–1309.
[25] Gaussian 09, Revision C.01, M. J. Frisch, G. W. Trucks, H. B. Schlegel, G. E. Scuseria, M. A. Robb, J. R. Cheeseman, G. Scalmani, V. Barone, B. Mennucci, G. A. Petersson, H. Nakatsuji, M. Caricato, X. Li, H. P. Hratchian, A. F. Izmaylov, J. Bloino, G. Zheng, J. L. Sonnenberg, M. Hada, M. Ehara, K. Toyota, R. Fukuda, J. Hasegawa, M. Ishida, T. Nakajima, Y. Honda, O. Kitao, H. Nakai, T. Vreven, J. A. Montgomery, Jr., J. E. Peralta, F. Ogliaro, M. Bearpark, J. J. Heyd, E. Brothers, K. N. Kudin, V. N. Staroverov, R. Kobayashi, J. Normand, K. Raghavachari, A. Rendell, J. C. Burant, S. S. Iyengar, J. Tomasi, M. Cossi, N. Rega, J. M. Millam, M. Klene, J. E. Knox, J. B. Cross, V. Bakken, C. Adamo, J. Jaramillo, R. Gomperts, R. E. Stratmann, O. Yazyev, A. J. Austin, R. Cammi, C. Pomelli, J. W. Ochterski, R. L. Martin, K. Morokuma, V. G. Zakrzewski, G. A. Voth, P. Salvador, J. J. Dannenberg, S. Dapprich, A. D. Daniels, Ö. Farkas, J. B. Foresman, J. V. Ortiz, J. Cioslowski, and D. J. Fox, Gaussian, Inc., Wallingford CT, 2009
[26] T. Spalek, P. Pietrzik, J. Sojca, J. Chem. Inf. Model. 45 (2005) 18–29.
[27] L.A. Bruno, B.M. Su, Appl. Spectrosc. 51 (1997) 755–758.
[28] D.G. Pobedimskii, Sh.A. Nasybullin, P.A. Kirpichnikov, R.B. Svitych, O.P. Yablonskii, A.L. Buchachenko, Organic Magnetic Resonance 9 (1977) 61–63.
[29] D.W. Bennett, T.A. Siddiquee, D.T. Haworth, S.V. Lindeman, J. Chem. Cryst. 37 (2007) 207–212.
[30] D.M. Murphy, I.A. Fallis, R.D. Farley, R.J. Tucker, K.L. Avery, D.J. Willock, Phys. Chem. Chem. Phys. 4 (2002) 4937–4943.
[31] M. Hoshino, A. Sekine, H. Uekusa, Y. Ohashi, Chem. Lett. 34 (2005) 1228–1229.
[32] S.F. Tayyari, M. Vakili, A. Nekoei, H. Rahemib, Y.A. Wang, Spectrochimica Acta Part A 66 (2007) 626–636.
[33] K. Nakamoto, Y. Morimoto, A.E. Martell, J. Am. Chem. Soc. 83 (1961) 4533–4536.
[34] R.C. Fay, T.J. Pinnavaia, Inorg. Chem. 7 (1968) 508–514.
[35] I. Diaz-Acosta, J. Baker, J.F. Hinton, P. Pulay, Spectrochimica Acta Part A 59 (2003) 363–377.
[36] B. Vlčková, B. Strauch, M. Horák, Coll. Czech. Chem. Comm. 52 (1987) 686–695.
[37] W. Linert, E. Herlinger, P. Margl, R. Boča, J. Coord. Chem. 28 (1993) 1–16.
[38] I. Bernal, P.H. Rieger, Inorg. Chem. 2 (1963) 256–259.
[39] C.J. Ballhausen, H.B. Gray, Inorg. Chem. 1 (1962) 111–122.
[40] J. Selbin, Chem. Rev. 65 (1965) 153–175.
[41] E. Garribba, G. Micera, A. Panzanelli, Inorg. Chem. 42 (2003) 3981–3987.
[42] D. Mustafi, M.W. Makinen, Inorg. Chem. 44 (2005) 5580–5590.
[43] M. Rangel, A. Leite, M.J. Amorim, E. Garribba, G. Micera, E. Lodyga-Chruscinska, Inorg. Chem. 45 (2006) 8086–8097.
[44] J. Costa Pessoa, I. Cavaco, I. Correia, I. Tomaz, T. Duarte, P.M. Matias, J. Inorg. Biochem. 80 (2000) 35–39.
[45] B.D. Howes, C. Kuhlmeyer, R. Pogni, R. Basosi, Magn. Reson. Chem. 37 (1999) 538–544.
[46] M.W. Makinen, M.J. Brady, J. Biol. Chem. 277 (2002) 12215–12220.
[47] J.P. Costes, F. Dahan, B. Donnadieu, J. Garcia-Tojal, J.P. Laurent, Eur. J. Inorg. Chem. (2001) 363–365.
[48] N.D. Chasteen, in: L.J. Berliner, J. Reuben (Eds.), Biological magnetic resonance, vol. 3, Plenum Press, New York, 1981, pp. 53–119.
[49] T.S. Smith II, R. LoBrutto, V.L. Pecoraro, Coord. Chem. Rev. 228 (2002) 1–18.
[50] S. Gorelsky, G. Micera, E. Garribba, Chem. Eur. J. 15 (2010) 8167–8180.
[51] K.H. Thompson, C. Orvig, Dalton Trans. (2000) 2885–2892.